Chapter 2

THE DEVELOPMENT OF AN EXPERIMENTAL DEVICE TO STUDY ELASTIC PROPERTIES UNDER HIGH PT CONDITIONS

Today, several different experimental set-ups are established to determine *in-situ* physical properties of rocks as a function of pressure *P* and temperature *T*. Two different pressure systems are used for experiments at *T* higher than 200 °C: mechanical presses, operating with a solid pressure medium and gas-pressure vessels. Fig. 2.1 illustrates the relation between *PT* range and possible sample geometries for a number of ultrasonic set-ups, described in the literature for both mechanical presses and gas-pressure vessels [see Ref. in Fig. 2.1]. Obviously the parameters pressure, temperature, and sample size interact in a complex way. In comparison to gas-pressure vessels, mechanical presses are capable for operations at higher pressures (2 GPa). However, with increasing pressure a substantial reduction of the sample size has to be accepted. Gas-pressure vessels are usually operated between 0.2 and 1 GPa; the realisation of pressures up to 2.5 GPa is rather an exception [Müller & Massonne, 2001]. Gas-pressure vessels provide the possibility to work at higher temperatures (1400 °C). However, the increase of temperature is realised again at the expense of the sample diameter, which is a major drawback of many existing ultrasonic set-ups. Too small sample sizes may lead to serious problems when interpreting ultrasonic data (see Chapter 2.4).
On the basis of the utilisation of larger, encapsulated samples, a new ultrasonic set-up was developed, for which the requirements can be summarised as follows:

- A high confining pressure (750–900 MPa) should prevent thermal microcracking.
- To observe dehydration reactions in silicates, temperatures above 500 °C are needed.
- The velocity of an elastic wave is highly dependent on the temperature of the transmitted medium.

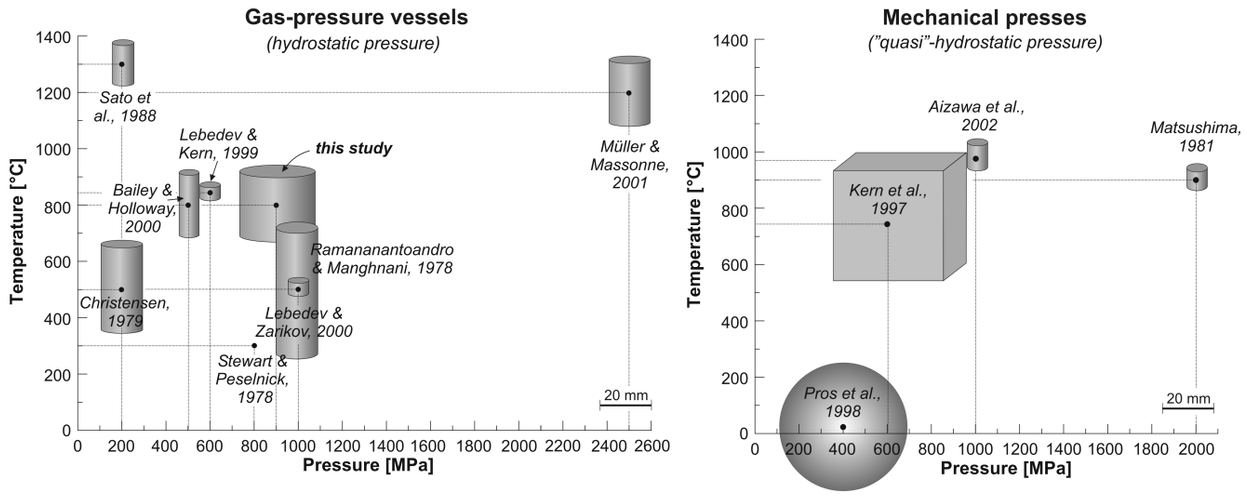

Figure 2.1: *The correlation between the parameters pressure, temperature, and sample dimension. The data display a compilation of different ultrasonic set-ups described in the literature.*

The reduction of a thermal gradient inside the sample to the greatest possible extent is thus of fundamental relevance for the careful conduction of adequate high temperature – ultrasonic experiments.

- The samples must be encapsulated fluid-tight up to the confining pressure, to guarantee undrained experimental conditions.

- The utilisation of relatively large samples was aspired, as this would reduce negative boundary effects during ultrasonic measurements, such as grain size effects, sidewall reflections or the generation of bar waves instead of body waves.

- To improve the quality of ultrasonic data the noise level should be reduced effectively.

Due to the extreme experimental conditions all components are exposed to considerable forces. Within the framework of this thesis, a number of materials and set-ups were tested, to develop an efficient experimental arrangement, capable of the measurement of P and S wave velocities under high *PT* conditions on relatively large samples (Fig. 2.1). In the following, a general overview of the final set-up is given, completed by the description of some details of the design and operation of its individual components.

2.1 The Experimental Set-up

To determine elastic wave velocities of rock samples under high pressure and temperature, the ultrasonic experiments are conducted in an internally heated gas-pressure vessel (Harwood). The fluid medium argon can be compressed to a maximum hydrostatic pressure of 1 GPa (10 kbar), which corresponds to a depth of about 30 km in the Earth‘s interior. The developed furnaces reach a temperature of up to 800 °C. The set-up is composed of a cylindrical rock sample (25 mm in length; 29.5 mm and 24.5 mm in diameter, respectively), which is placed between two buffer rods of a sintered Al_2O_3-ceramic, with a corresponding diameter, and usually 58 mm in length (Fig. 2.2). To ensure an optimal contact between sample and buffer rods, which is required especially at low confining pressure, the surfaces of the sample as well as those of the buffer rods were polished. P and S wave transducers with resonance frequencies of 1 or 2 MHz are glued on the ends of the buffer rods. To avoid uncontrolled draining of fluids during the experiment, the internal ultrasonic set-up is mantled with a Ni-alloy steel tube (Ni-alloy jacket in Fig. 2.2). Its ends are sealed with a small amount of epoxy resin. Hence, while the pressure is build up in the vessel, no gas can enter the tube. The increasing gas-pressure, therefore, presses the tube

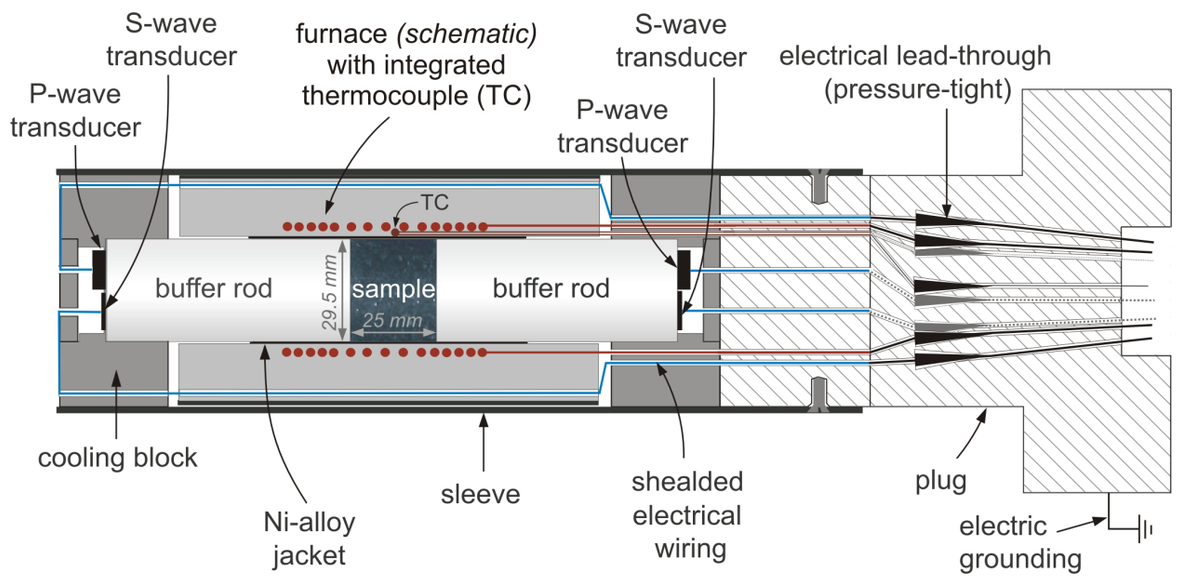

Figure 2.2: *The experimental device (schematic). The internal ultrasonic set-up consists of a sample, two buffer rods, and ultrasonic transducers and is encapsultated in a Ni-alloyed steel tube. The furnace is a 6-zone resistance heating element with an integrated thermocouple (TC). The points schematically indicate the varied heating power of the furnace, with a reduced heating capacity in its central part to achieve a balanced T-profile over the sample. During the heating experiment the transducers are cooled by blocks of massive brass. The plug holds 8 to 10 pressure-tight electrical lead-throughs, arranged in a circle. They constitute the interface of communication between the outer controlling units and the experimental set-up in the vessel.*

gas-tight onto the set-up. In consequence, the sample is quasi-encapsulated at self-sealing conditions and represents a ”closed”, *undrained* system as long as the internal fluid pressure is smaller than the confining pressure. To reduce the amount of carbon in the high temperature area the tube is sealed at the coldest, outer part of the assembly to effectively eliminate a carbon contamination of the sample during the experiment.
The set-up is placed in a bifilar 6-zone furnace to reduce temperature gradients in the sample. To avoid an overheating of the transducers, the ends of the buffer rods are attached to cooling blocks of massive brass, which in turn are in contact with the cooling system of the pressure vessel. Finally, the whole arrangement is fixed on the closure plug and placed in the autoclave. The electrical insulation of the lead-throughs was optimised by the *High Pressure Development Lab* of the GFZ for high frequency use to reduce reflections of the signals in the plug.

2.2 The Gas-Pressure Vessel

The used Harwood autoclave (Fig. 2.3) consists of a cylindrical vessel. At both sides, plugs with the sealing package are placed in the vessel and fixed with unwieldy screws. The pressure inlet is realised through one of these plugs. The other one is designed to lead the electrical connections from inside the autoclave outwards. Thus, once the set-up is installed inside the vessel, the experiment can only be controlled by lead-throughs, which allow heating, controlling of temperature, and the conduction of ultrasonic measurements. In the original design the plug incorporates 8 lead-throughs, where the transducers (1 lead-through per transducer plus ground), the thermocouple (2 lead-throughs per thermocouple) and the furnace (at least 2 lead-throughs) are connected. Hence, the set-ups were equipped with 2 P wave and 2 S wave transducers. To preserve the strength of the steel, the vessel is provided with an external water-cooling system. In the course of this study, two times the cone of an electrical lead-through blew off from its seat in the plug, each time at $P > 900$ *MPa* (blow-out). After the second blow-out the *High Pressure Development Lab* of the GFZ re-designed the plug and other accessories to substantially reduce the accident risk. The new plug now contains 10 lead-throughs (2 P and 4 S wave transducers). Therefore, the last experiments could be performed with two additional transducers.
The above mentioned blow-outs had a considerable influence on the experiments. Before the first blow-out the pressure vessel was almost perfectly sealed. With the sealing package having been re-designed by the GFZ workshop the pressure loss from a starting value of 1 GPa was about 30 to 40 MPa in 16 hours. Under this condition the pressure was built up in steps of 10 MPa (100 bar) up to 100 MPa, and 20 MPa up to 200 MPa. Between 200 and 1000 MPa the increments were 50 MPa. After adjustment of each pressure step, up to 45 min elapsed before the measurement of elastic wave travel-times were started to equilibrate the sample. Before starting the temperature experiment, the pressure was slowly

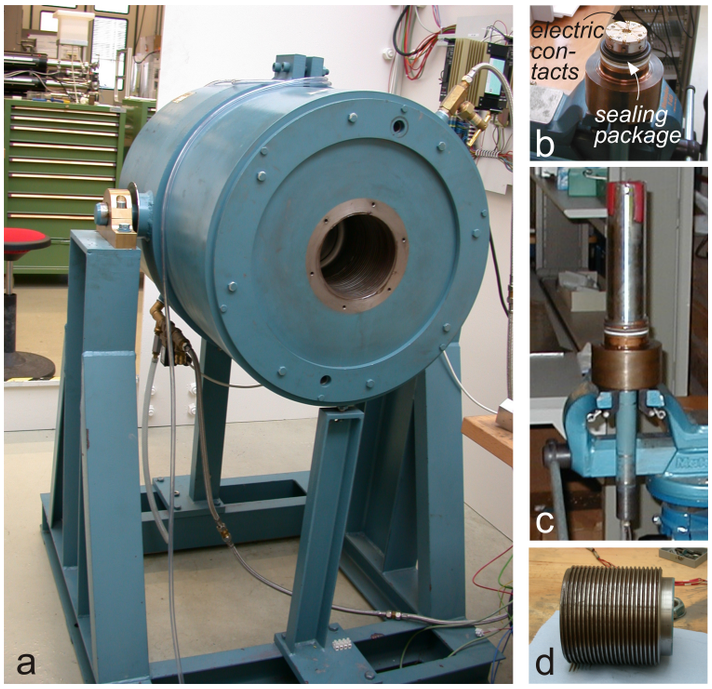

Figure 2.3: *The gas-pressure vessel (Harwood) and its accessories. (b) The closure plug with sealing package. The electric connections are arranged circularly. (c) Closure plug with the experimental set-up. (d) The closure screw.*

reduced to about 900 MPa due to safety considerations.

After the blow outs of the autoclave, the sealing of the vessel, especially at pressures higher than 500 MPa became worse and the pressure program had to be shortened to a few pressure steps. Because of the pressure loss, the T–experiments were performed at slightly reduced pressures between 750 and 850 MPa. To achieve best possible constant P conditions the pressure was regulated continuously. With increasing temperature the pressure loss was compensated by the thermal expansion of the fluid medium.

2.3 The Heating Device

A very delicate component of ultrasonic devices in gas-pressure vessels is the furnace. It is placed inside the vessel and is thus exposed to the same pressure as the sample. Unfortunately, the furnace components react very sensitively to the extreme pressure conditions in the highly mobile convecting pressure medium. Thus, furnaces tested at ambient conditions (P = 1 bar) up to temperatures of 1200 °C, already failed at 700 °C or even 500 °C, when operated under pressure of $\sim$ 900 *MPa*. Therefore a number of materials and furnace concepts were tested in this study: Due to the limited volume in an internally heated pressure vessel, an obvious general rule is: the higher the maximum working temperature, the smaller is the hot volume. This rule is dictated by the limited power capacity of the lead-throughs as well as the heater elements and the necessities to cool the inner wall of the autoclave and to minimise

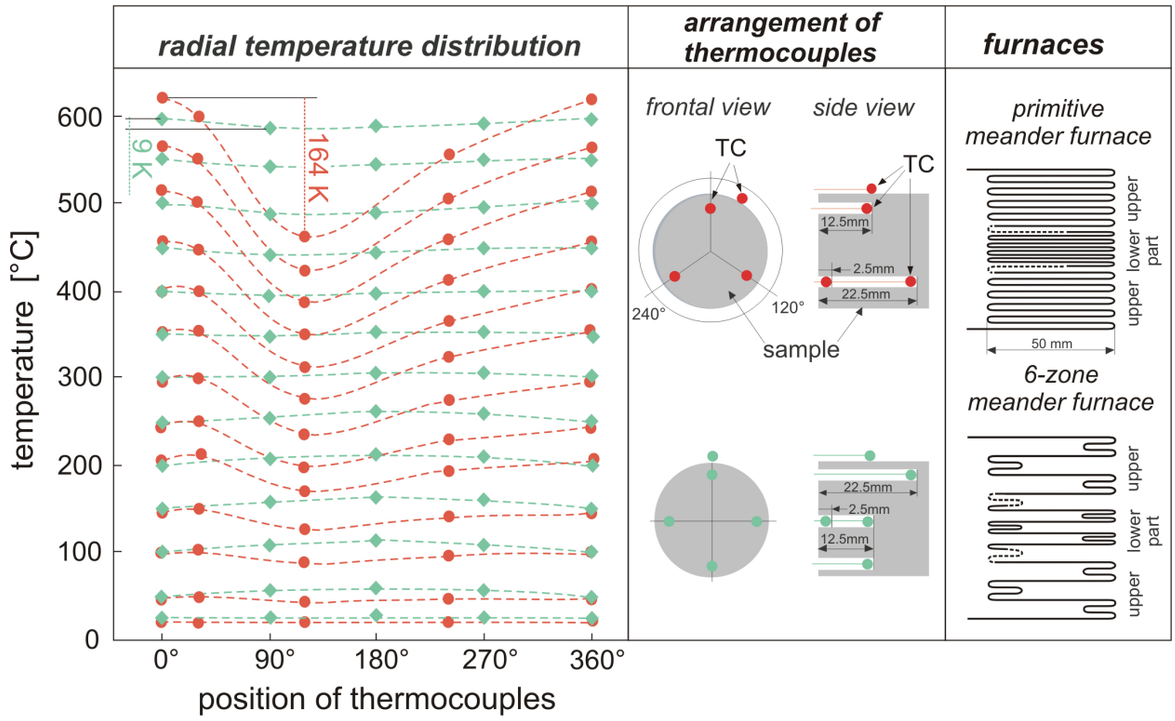

Figure 2.4: *Radial temperature distribution in the autoclave for two different resistance furnace configurations, which are shown schematically on the right. The furnaces are tested with 4 and 5 thermocouples (TC), respectively. The arrangement of the thermocouples in the sample is illustrated. Red: data for a primitive meander furnace; blue: data for a 6-zone meander furnace.*

the convection inside the autoclave. Therefore, thermal insulation has to be optimised, especially for elevated temperatures. Another important aspect is the effective reduction of thermal gradients. In a gas medium pressure, the temperature distribution is established mainly by convecting gas. The rise of heat in the autoclave leads to stronger heating efficiency in the upper part than in the lower one. To utilise the convective heat transport to achieve a radially symmetrical thermal gradient, conventional experimental devices are normally in a vertical position. For this reason, the furnaces are generally cylinders closed at the top and slipped over the set-up. However, for reasons given in section 2.8, the measurements in this study had to be performed with ultrasonic transducers arranged on both ends of the set-up. This in turn requires a horizontal position of the whole experimental device to avoid an overheating of the transducers. Therefore, one challenge of this study was, to construct a furnace with the smallest possible radial and lateral temperature gradients throughout the largest possible sample volume.

Different concepts of furnaces were tested, modified, and optimised. To control the furnaces Ni/ NiCr–thermocouples were used, which were integrated in the furnace and thus placed upon the surface of the specimens. For furnace calibration further Ni/NiCr-thermocouples were installed in the interior of the specimen to compare the temperature distribution inside the sample with the temperature of the furnace

(Fig. 2.4). The heating program follows a ramp scheme, e.g. the sample is heated in increments of 50 K. At each 50 K step it was tested, how long a hold must be, to ensure thermal equilibration of the sample. Three and four Ni/NiCr-thermocouples, were countersunk to different depths in an area of 25 mm length in the middle of the test cylinders, which represents an idealised sample – rods assemblage. To arrange the experimental conditions as similar as possible to ultrasonic measurements, the set-up to determine the thermal gradient was jacketed with a Ni-alloy tube and put into the cooling blocks.
Furnaces available for internally heated pressure vessels are all based on a resistance design and utilise the heating of current conductors. In the classical design, temperature gradients are compensated by the use of two- to three-zone furnaces, consisting of two and three seperately operated heating elements, respectivley. However, the general conceptual design of the furnace is limited by the restricted number of electrical lead-throughs of the autoclave. In this study 8 to 10 lead-throughs were available for the whole experimental set-up. This is not enough to utilise a classical two- or three-zone furnace. Thus, furnaces were built of a continuous 0.5 mm thick, hot drawn NiCr-wire (Kanthal), with one end defined as the electrical bonding. Unlike radially wound furnaces, the wire meanders over the set-up to exploit the advantage of the fact that the heating power can be controlled by the tightness of the meanders. Fig. 2.4 shows the temperature distribution up to temperatures of about 600 °C measured with different modifications of a meander furnace. The red dataset belongs to a primitive meander furnace. In the optimised furnace most of the windings concentrate in the lower part of this furnace to compensate for the vertical thermal gradient. However, the temperature distribution from the middle of the sample to its ends is extremely inhomogeneous. To compensate for this lateral thermal gradient, additional shorter meander-windings double the heating power at the end of the furnace. As shown in Fig. 2.4, the usage of a 6-zone meander furnace provides to a nearly balanced temperature field around the sample. This arrangement reduces the thermal gradient from 164 K to 9 K at 600 °C over the entire sample of 25 mm in length and 29.5 mm in diameter.

A fundamental problem in operating a resistence furnace under high gas pressure is that the wire tends to evaporate at its hottest parts, because of the extreme convection of the pressure medium. In case of the meander furnace the hottest parts are the loops, where the wire is stressed exceedingly by bending. To minimise the risk of burning out, the wire is fixed completely with Ceramabond 256, an adhesive on Al_2O_3 basis. To assure a thermal insulation against the autoclave wall, the space between heating element and outer furnace sleeve was filled with Al_2O_3-insulation padding. The electrical leadings of the transducers from the backside of the set-up run directly under the outer furnace sleeve and are therefore in the cooled zone of the furnace. The furnaces reach temperatures of 700 to 800 °C, because the samples are relatively large. To reach higher temperatures a high-temperature set-up using a sample with a diameter slightly reduced to 24.9 mm was developed, to enhance insulation with minimum loss of sample volume.

2.4 The Buffer Rods

Buffer rods are integrated into the set-up to keep the temperature-sensitive ultrasonic transducers off the hot zone. The second function of the buffer rods is the gas-tight connection with the steel tube, for encapsulating the sample. Three materials for the rods were tested: a ZrO_2-ceramic, SiO_2-*glass*, and an Al_2O_3-ceramic. The crucial factors for their choice were their low thermal conductivity, their relatively low attenuation of elastic waves, and low reactivity with the sample. A number of tests were conducted to determine the range of dimensional restrictions of the sample assembly, the general measurement set-up, and the chemical and mechanical stability of the rods under experimental *PT* conditions.

In a first test series (Fig. 2.5) the signal quality was optimised with regard to its dependence from the diameter of the sample assembly, the frequency of the used transducers, and the grain size of the sample. Generally, high temperature–ultrasonic assemblies resemble rather a cylindric bar than an infinitely extended body, because the dimensions of the rods ($d = 29.5$ *mm*; $l = 58$ *mm*) are restricted by the size of the working cavity of the pressure vessel on the one hand, and the need of cool rod ends on the other. In dependence of the selection of the length *l*, diameter *d* and frequency *f*, not only the direct wave (black arrows), but also sidewall reflections occur. At unfavourable dimensions of the sample assembly the direct phase may be superimposed by the sidewall reflections or submerge into the noise. In the worst case, dilation, as it appears at the passage of a compressional wave, induces a lateral contraction, which is known as bar wave ($v_b = \sqrt{\frac{E}{\rho}}$). To minimise these effects often certain *length-to-diameter ratios (l/d)* or *diameter-to-wavelength ratios (d/*λ*)* are considered [Anderson & Liebermann, 1968 and references therein]. Tests reveal that the *l/d* ratio is less important for determining sound velocities: The number of sidewall reflections increases with increasing *l/d* ratio, but the observed traveltimes are not influenced. Furthermore a linear d/λ ratio of ≥ 5 is recommended, which is deduced from $\lambda = v/f$ (light-grey dashed lines in Fig. 2.6). Regarding this ratio the utilisation of high velocity materials, such as Al_2O_3 (v_p = 10.3 km/s), would be rather impossible in internally heated gas-pressure vessels, because a minimum sample diameter of 50 mm would be required if 1 MHz transducers are used. Fig. 2.5 summarises test measurements on high (Al_2O_3: v_p = 10.3 km/s) and medium (Al: v_p = 6 km/s) velocity materials. The rods had a fixed length of 60 mm, but varying diameters. P waves of diverse frequencies, namely 1, 2, and 4 MHz, were induced in the rods, reflected at the backside and recorded with the transducer:

For medium velocity materials (*Al*) the sidewall reflections occur in larger time intervals compared to high velocity materials (Al_2O_3) and converge, independently from the material, to the direct wave as the diameter decrease. Under the assumption of a linear relation between the diameter and the wavelength the d/λ ratio should be independent from the investigated material. However, the tests suggest that the introduction of a critical *diameter-to-wavelength* ratio is unsuitable at all to deduce a valid set-up geometry from it. Rather the relation between sample diameter and wavelength can be described in a first

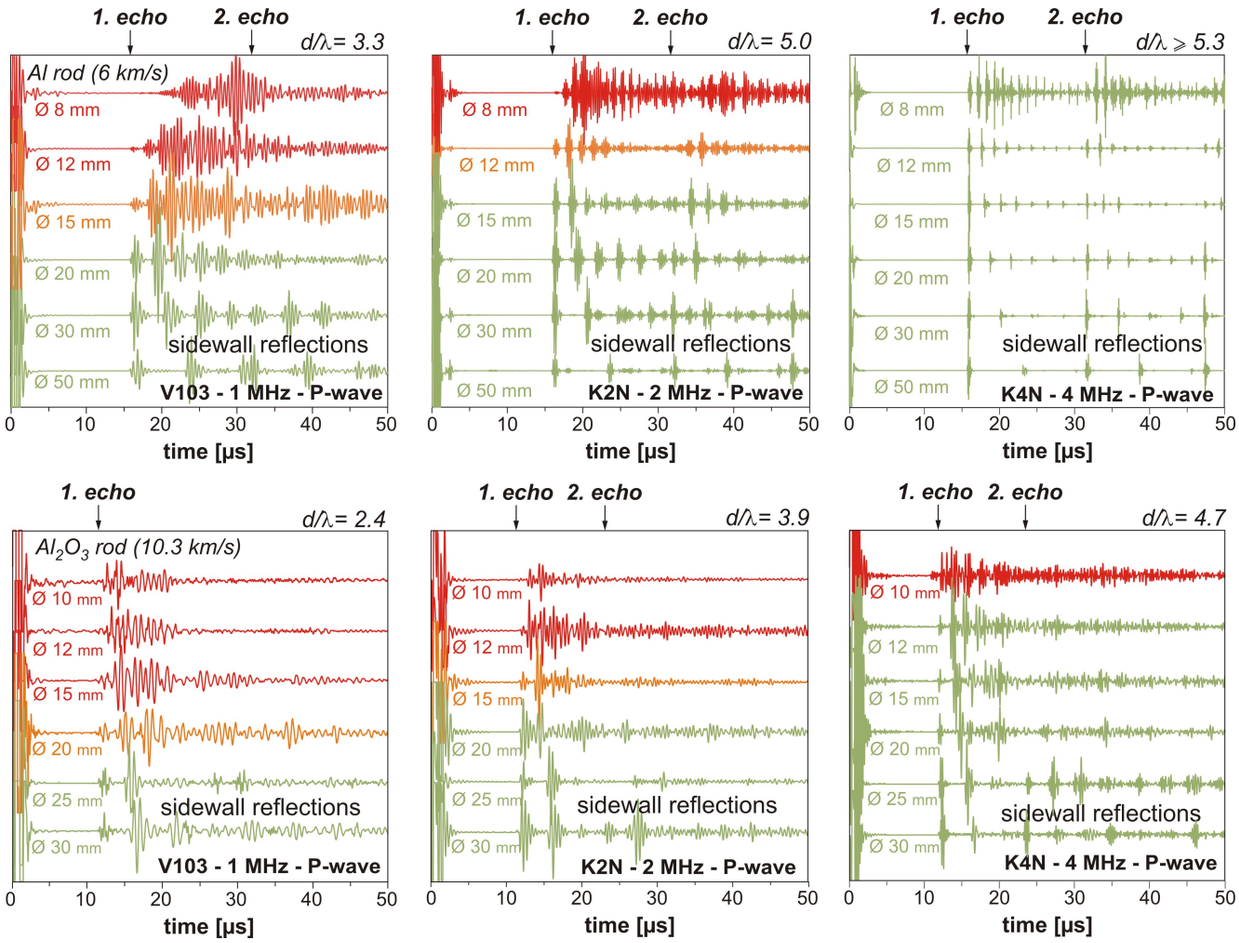

Figure 2.5: *P wave signals were determined at 1 MHz, 2 MHz, and 4 MHz. A strong relation between signal quality, sample geometry, and the material of the rod is evident. The frequency of the P waves and the diameter of the sample are responsible for a number of sidewall reflections. The quality of the P wave signals was used to derive the critical diameter to wavelength ratio (d^2/λ; Fig. 2.6). (Traveltime boxes in the upper line were taken from Schilling & Ramelow [2001].)*

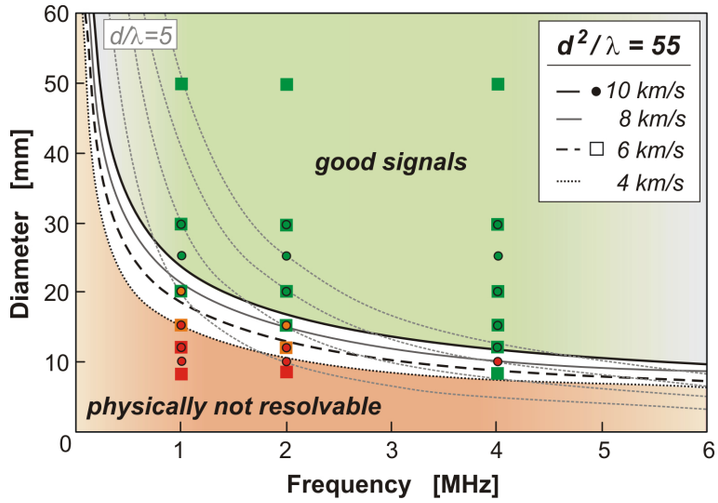

Figure 2.6: *For a given P wave velocity the minimum utilisable diameter of the sample depends on the applied frequency. The diagram is derived for diverse velocities from a critical d^2/λ ratio of 55. Squares and points mark the diameters of Al and Al_2O_3 rods, respectively, which were tested in Fig. 2.5 for different frequencies. Dashed lines in light-grey refer to a linear d/λ-ratio of 5 [Anderson & Liebermann, 1968].*

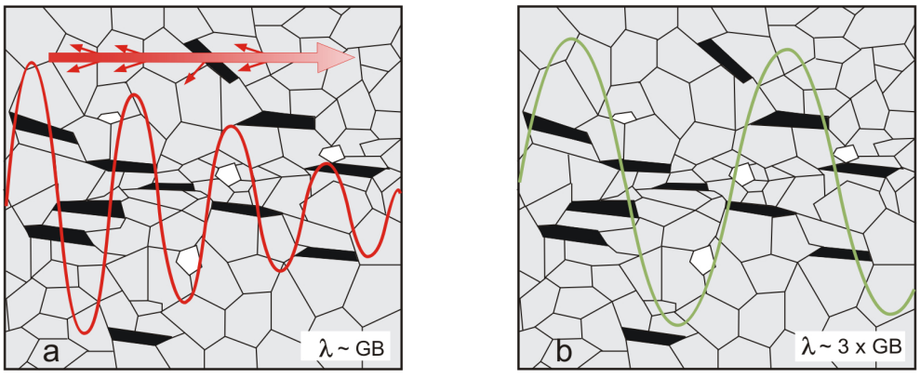

Figure 2.7: *Grain boundaries (GB) represent interfaces at micrometer scale. (a) When using a frequency with the wavelength λ in the dimension of the grain size, the signal will be strongly attenuated due to scattering of energy at each interface. (b) To reduce the attenuation λ should be at least three times the grain size.*

approximation by d^2/λ, in order to have a sufficient control on the onset of the direct phase (Fig. 2.6). The transition between good and non-analysable signals is smooth and from the test series an empiric d^2/λ of $\sim$ 50 to 60 was found. As a consequence of these tests it must be assumed that experiments with a small diameter – set-up used for natural rock samples [e.g. Sato et al., 1988; Bailey & Holloway, 2000; Lebedev & Zarikov, 2000/ compare with Fig. 2.1] move out off the limits of physical possibility [Schilling & Ramelow, 2001].

By utilising higher frequencies, the wave field becomes generally more clear and even multiple echos can be identified. However, the materials tested in Fig. 2.5 are micro-crystalline (Al_2O_3, ZrO_2) and amorphous (SiO_2), respectively. Therefore, the attenuation of the signals is weak, and signal to noise ratio and thus the data quality is high. On the other hand, in a natural rock sample, characterised by a larger grain size and including pores and cracks, high frequencies are affected by a stronger damping. The upper boundary of an adequate frequency-value is therefore limited by the microstructure of the sample, as illustrated schematically in Fig. 2.7 for a polycrystalline rock with a certain grain size. In the case of the transmission of an ultrasonic signal with a wavelength λ corresponding to the grain size, the signal will be strongly attenuated, as energy will be scattered at the interfaces (such as grain boundaries, pores, and cracks) and the pulse becomes distorted [e.g. Mason & McSkimin, 1947]. To limit the attenuation, the experiments were conducted with transducers of 1 MHz resonance frequency, which ensure that λ is at least 3 times larger than the grain-size of the rock, which is usually seen as the minimum wavelength, if bulk properties are to be determined [Gebrande, 1982]. Some experiments were performed with 2 MHz tranducers. In these cases a slight signal attenuation was accepted in favour of sharper signals, which are better seperated from sidewall reflections.

In general, two different measurement set-ups are established for laboratory experiments. In a *transmission set-up* one ultrasonic transducer sends an elastic wave through the sample–buffer rod-assembly,

which is recorded with a second transducer at the opposite end. In a *pulse–echo arrangement* only one transducer is needed to transmit an elastic wave and receive its echos, reflected at each interface of the assembly (*buffer rod–sample interface (1. echo)/ sample–buffer rod interface (2. echo)*). The benefit of the second method is that it minimises the number of transducers and thus the number of electric lead-throughs needed, and that only the end with attached transducers has to be cooled, which reduces the complexity of the furnace.

For the tested sample–buffer rod systems the *reflection coefficient R*, which is a measure of the impedance contrast between buffer rod and sample is calculated from:

$$R = \frac{\rho_2 v_2 - \rho_1 v_1}{\rho_2 v_2 + \rho_1 v_1} = \frac{Z_2 - Z_1}{Z_2 + Z_1}, \tag{2.1}$$

where Z_1 and Z_2 are the acoustic impedances of the first and the second transmitted medium, defined by the corresponding product of density ρ_i and velocity v_i [Telford et al., 1990]. The results are summarised in Tab. 2.1. For Al_2O_3 and ZrO_2 the *rod–amphibolite* reflection coefficients for both, P and S waves are on the order of about -0.40 (P waves) and -0.35 (S waves). From these values it can be derived that the amplitude of the first echo, reflected at the *buffer rod – sample* interface is reduced by about 60 % and 65 % of the amplitude of the incident wave, respectively. The echo reflected at the second sample – buffer rod interface contains still 14 to 15 % of the incident amplitude and should be resolvable in pulse-echo seismograms. However, tests reveal when utilising ZrO_2 as well as Al_2O_3, both P and S wave

	first medium		*second medium*			*residual amplitude [%]*	
	ρ $[g\ cm^{-3}]$	$\mathbf{v_p}$ $[km\ s^{-1}]$	ρ $[g\ cm^{-3}]$	$\mathbf{v_p}$ $[km\ s^{-1}]$	**R**	**echo I**	**echo II**
Al_2O_3 – amphibolite	3.84	10.3	2.82	6.35	-0.3767	37.67	14.63
Al_2O_3 – serpentinite	3.84	10.3	2.88	7.52	-0.2923	29.23	14.64
ZrO_2 – amphibolite	5.97	7.07	2.82	6.35	-0.4042	40.42	14.35
ZrO_2 – serpentinite	5.97	7.07	2.88	7.52	-0.3218	32.18	14.80
SiO_2 – amphibolite	2.23	5.87	2.82	6.35	0.1554	15.54	11.09
SiO_2 – serpentinite	2.23	5.87	2.88	7.52	0.2466	24.66	14.00
	first medium		*second medium*			*residual amplitude of [%]*	
	ρ $[g\ cm^{-3}]$	$\mathbf{v_s}$ $[km\ s^{-1}]$	ρ $[g\ cm^{-3}]$	$\mathbf{v_s}$ $[km\ s^{-1}]$	**R**	**echo I**	**echo II**
Al_2O_3 – amphibolite	3.84	6.01	2.82	3.74	-0.3576	35.76	14.76
Al_2O_3 – serpentinite	3.84	6.01	2.88	3.78	-0.3590	35.90	14.75
ZrO_2 – amphibolite	5.97	3.72	2.82	3.74	-0.3407	34.07	14.81
ZrO_2 – serpentinite	5.97	3.72	2.88	3.78	-0.3421	34.21	14.81
SiO_2 – amphibolite	2.23	3.65	2.82	3.74	0.1459	14.59	10.64
SiO_2 – serpentinite	2.23	3.65	2.88	3.78	0.1444	14.44	10.57

Table 2.1: *P and S wave reflection coefficients for different tested buffer rod – sample assemblies.*

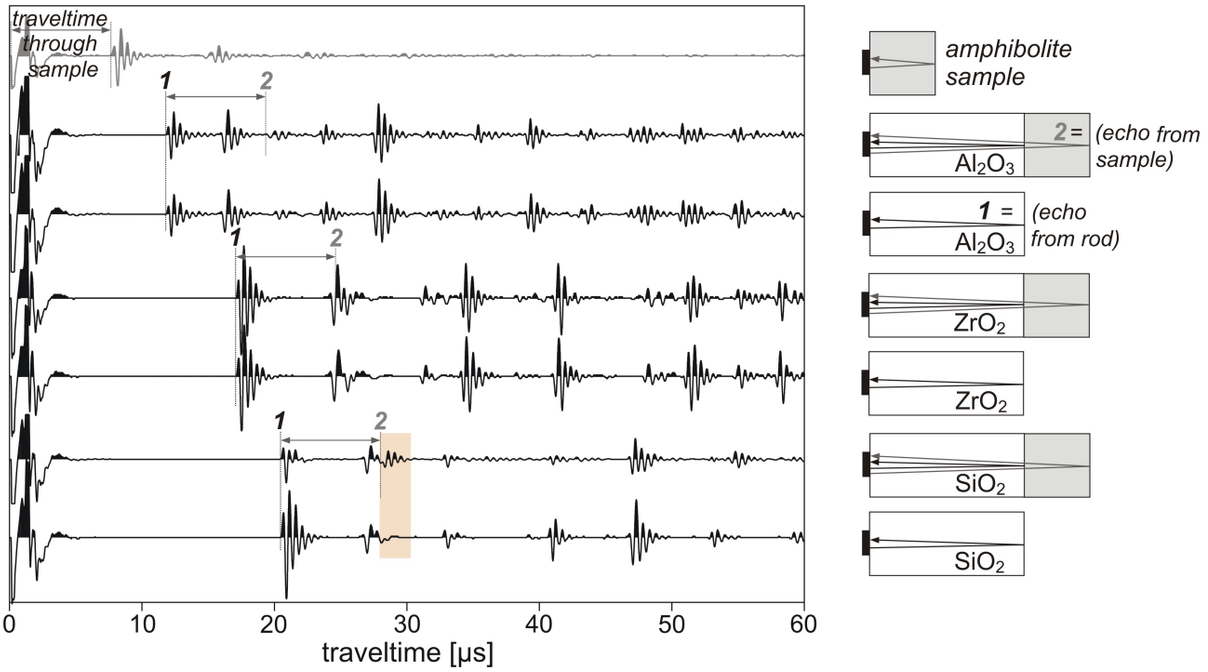

Figure 2.8: *Pulse echo–P wave seismograms for an amphibolite sample (uppermost trace), different buffer rod materials (Al_2O_3, ZrO_2, SiO_2), and corresponding buffer rod – sample systems. Onset* **1** *refers to the echo of the buffer rod back plane,* **2** *marks the theoretical onset of the echo from the sample back plane. Note that only for the system SiO_2-rod – sample an echo from the sample backside can be clearly identified, while for Al_2O_3 and ZrO_2 the recordings of the rods and the rods + sample are nearly identical and differ mainly in amplitudes. All traces were recorded with the same amplification.*

echos from the sample back surface are embedded into noise or superimposed by sidewall reflections and can not be analysed (Fig. 2.8). This may be attributed to the relatively large difference between the energy contents of the first and second echo in case of ZrO_2 as well as Al_2O_3, causing the low-energy phase to disappear in the noise. The P and S wave impedance contrasts of SiO_2-glass buffer rods and the samples are less pronounced, and result in an almost complete transmission of the energy through the whole sample assembly. Thus both relevant phases are characterised by low, but nearly equal energies. Therefore, using SiO_2-glass buffer rods the echo of the sample back side can be resolved in the tests (Fig. 2.8 - bottom lines). Hence, under the aspect of signal quality SiO_2-glass would be the ideal buffer rod material.

Regarding the stability criteria it turned out that ZrO_2 is chemically not stable under the experimental conditions and reacts with the Ni-alloy steel capsule. A possible explanation might be that ZrO_2 is stabilised by Ca. The required charge balance is achieved by oxygen vacancies, which, in turn, cause a high oxygen conductivity of the ZrO_2 ceramic [Schilling, 1991]. In the Ar-atmosphere of the autoclave the oxygene fugacity p_{O_2} is low and may lead to a reduction of ZrO_2 and finally to the melting of the Ni-alloy steel capsule, probably due to Zr – Ca – Ni - eutectic.

The SiO_2-glass rods, on the other hand, include small elongated air bubbles due to manufacturing shortcomings. The squeezing of these voids potentially leads to the cracking of the glass rods with increasing pressure. Thus, the aspired *"undrained"* experimental conditions could not be ensured as fluids may leak through the cracked buffer rod.

For the described reasons the experiments were conducted exclusively with Al_2O_3-rods, which are chemically and mechanically stable under the experimental conditions. However, in comparison to ZrO_2 and SiO_2-glass, Al_2O_3 has a relatively high thermal conductivity, which requires sufficient cooling of the ends of the rods, as the attached transducers are temperature sensitive. Moreover, caused by the unfavourable impedance contrast between buffer rod and samples, the experiments had to be conducted with transducers at each side of the set-up, which call for a horizontal position of the experimental device and hence the described careful calibration of the furnace. Another disadvantage of the used Al_2O_3 is its high P wave velocity of 10.3 km/s, which gives rise to short-interval sequence of signal and sidewall reflections. This in turn has an immediate influence on the data quality.

2.5 The Ultrasonic Device

To scale the measurement of elastic waves from field experiments to the laboratory at high PT, different frequency ranges are used (Fig. 2.9). According to P wave velocities in natural rocks of a couple of kilometres per second and natural/ artificial seismic frequencies between $\sim$ 0.1 and $\sim$ 1000 Hz the corresponding wavelengths vary between a few meters and several tenths of kilometers, respectively. Thus the experimental sample dimension in the lab is exceeded by orders of magnitude. Therefore, laboratory measurements of the propagation of body-waves are usually performed within the range of ultrasonic frequencies.

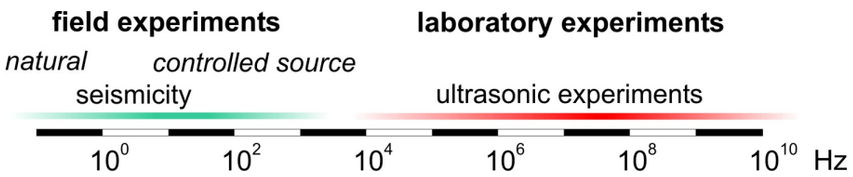

Figure 2.9: *Frequency ranges of seismological and seismic field experiments and laboratory measurements.*

The ultrasonic transducers and sensors used in this study consist of small discs (P wave) and plates (S wave) of a piezoelectric ceramic (Fuji Ceramic Corporation, PZT/ C6-material). The parallel surfaces of the transducer are sputtered with silver-electrodes, which serve as electrical contacts.

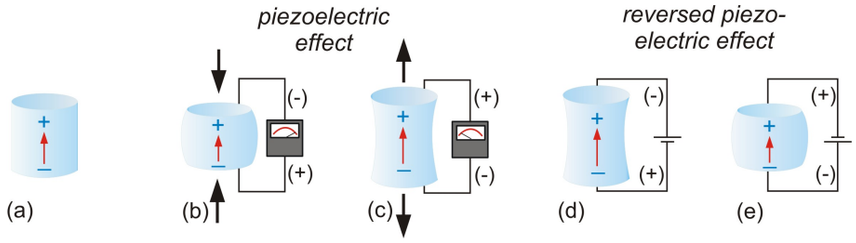

Figure 2.10: *The operating modes of piezoelectric transducers. (a) The transducer is made of a polarised, polycrystalline ceramic. Mechanical compression (b) or extension (c) of the piezoelectric element lead to the displacement of charges in the dipole domain of the transducer, which is reflected in the generation of a voltage (piezoelectric effect). The reversed piezoelectric effect (d and e) converts an electrical signal into mechanical energy. In dependence of the polarisation of the applied external voltage, the transducer is compressed or dilated. [after www.americanpiezo.com/piezo_theory/].*

The operation mode of ultrasonic sensors and transducers is based on the piezoelectric effect and its reversion (*electrostriction*), respectively. An electrical impulse causes a polarisation in the piezoelectric ceramic (*electrostriction*), which finally results in its mechanical deformation generating an elastic wave (Fig. 2.10 d and e). Depending on the polarisation of a voltage, the piezoelectric element is shortened or lengthened. An alternating voltage corresponding to the frequency of the mechanical Eigenschwingung of the piezoelectric *transducer* stimulates its resonance oscillation. The intrinsic piezoelectric effect, on the other hand, reverses this behaviour and converts the incoming elastic wave energy into an electrical signal (Fig. 2.10 b and c). Thus the piezoelectric element operates as a *sensor*. As both, the *sensor* and the *transducer* are physically the same element, in the following, only the term transducer is used, independent on the mode of operation.

The used Fuji transducers are made of a $BaTiO_3$ ceramic. Above a certain critical temperature, the Curie point, $BaTiO_3$ exhibits a cubic, perovskite-like symmetry and the barycentre of positive and negative charges lie in one point. At temperatures below the Curie point the $BaTiO_3$ lattice obtains a tetragonal symmetry accompanied by a dipole momentum. In the ceramic mass the polar domains are orientated randomly. To utilise the piezoelectric effect for technical application the polar domains of the polycrystalline material are aligned in a so-called poling treatment. For this, the ceramic is exposed to a strong, DC electric field during the cooling from above Curie temperature to room temperature, which confers a remanent polarisation of the ceramic. Depending on the orientation of the dipoles towards the transducer surface, P and S waves can be stimulated, respectively.

At temperatures approximately half-way between 0 °C and the Curie point, the polarised domains can become irreversibly disordered and the material might depolarise. With increasing temperature the conversion rate decreases and the signal to noise ratio increases. Thus, to avoid the overheating of the ultrasonic transducers during the experiment and the impairment of their operating ability, the transducers could not be placed directly on the sample (in the hot zone), but had to be mounted onto cooled

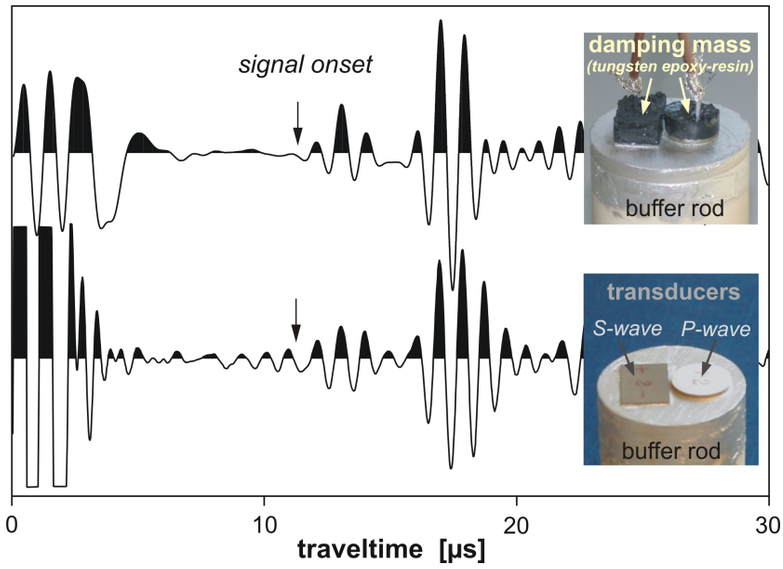

Figure 2.11: *The influence of sensor damping to signal quality. The bottom trace illustrate a strong ocillation of an undamped transducer in the pulse echo mode. The upper trace was recorded with a damped transducer. The damping material is a mixture of tungsten and epoxy resin. The arrows mark the signal onset.*

spacers (*buffer rods*) of a material with a low thermal conductivity. Materials with a higher Curie temperature (e.g. turmaline) were not considered as transducers, as they show a much weaker signal to noise ratio and a worse conversion ratio.

P as well as S wave transducers with a resonance frequency of 1 or 2 MHz are integrated in the set-up. The transducers are attached with a silver-alloy epoxy resin onto the buffer rods. Teflon masks were made to orientate the transducers during the glue procedure. The fixed side of the transducers is electrically grounded through the brass cooling blocks and pressure vessel. To reduce electomagnetic induction, the upper side of the transducers is contacted with a shielded cable (BNC) to receive and emit high-frequency electrical signals. To complete the electric shielding of the ultrasonic device the transducers extend into the cooling blocks of brass, which serve additionally as a Faraday cage.
A further enhancement of signal quality is reached by damping of the transducers. Without damping the oscillation of the transducer continues for several μs and may interfere with the signal from the sample (Fig. 2.5). To suppress the ringing and to record short, sharp signals, a 50 Ω resistance was connected in parallel to the transducers. Additionally, in the first set-ups the transducers were damped with plates of neoprene, which were pressed between the transducer and the lid of the cooling block. A number of different other electronic and mechanic damping methods, including the combination of inputsignal–inversed input signal and the use of springs between cooling block lid and transducers, were tested. However, the best damping was achieved when covering the transducers with a highly viscose mixture of tungsten powder ($\rho = 19.25\, g/cm^3$) and epoxy resin. The connection of the upper side of the transducers with their grounded side by the tungsten-epoxy mixture has to be avoided as short-circuits were observed.